Simulation Study on Robot Calibration Approaches

Pavel Kozlov[a] and Alexandr Klimchik[b]
Innopolis University, Innopolis, Russian Federation

Abstract: The paper compares elastostatic calibration approaches for serial industrial robots. Specifically, this paper compares identification strategies based on the different measurement point locations and data fusion algorithms. The paper analyzes several robot calibration hypotheses based on different robot models. All the hypotheses were tested in a simulation study with 1000 data sets. The results showed that "4-6DoF after 6+3DoF" and "3+6DoF comb" methods demonstrated the best results for the considered methods. Strategies were at least 1.86 times more accurate for the resulting deviation metric than the classical "6DoF" identification.

1 INTRODUCTION

Robots are widely used in assembling, welding, and machining operations (Nubiola and Bonev, 2013; Wu et al., 2015a; Qin et al., 2016). These operations require high positioning accuracy during the technological processes (Park et al., 2012). Consequently, the final product accuracy is strictly dependent on the robot accuracy. Therefore, a robot should be accurate enough. Unfortunately, robots make position errors which decreases the required accuracy. To solve this issue, some calibration technique must be provided (Li et al., 2021).

Robot calibration might be classified into geometric (Kamali and Bonev, 2019) and elastostatic calibration (Klimchik et al., 2017). Traditionally, positioning errors are assumed to be mostly provided by geometric errors (Wu et al., 2015b; Elatta et al., 2004). These errors are mainly introduced by links length and joint offsets which are constant values. These values do not depend on robot configuration or any external loading. The scientific community developed certain techniques to reduce such errors and almost ignore any geometric factors (Daney and Emiris, 2001; Driels et al., 1993; Veitschegger and Wu, 1987; Hage, 2012; Renders et al., 1992).

Another source of errors are the elastostatic problems. These problems arise during any technological process and depend on robot configuration and ex-

ternal load (Ma et al., 2017). Elastostatic errors appear in addition to the geometrical ones and may have higher impact on the resulting accuracy on different operations, milling for instance (Klimchik et al., 2016). Nevertheless, these errors can be also reduced. The reduction might be done by selecting an appropriate model and error compensation approach (Nguyen et al., 2022; Klimchik et al., 2014; Gonzalez et al., 2022).

From our experience, model parameters have different impact on the positioning accuracy (Klimchik et al., 2015). Therefore we can reduce the model to achieve robot accuracy with lower model complexity (Mamedov et al., 2018). Importantly, such a model must have only significant parameters (Klimchik et al., 2015). Numerous research might help to reduce model complexity within required robot calibration accuracy (Joubair et al., 2012; Jin and Gans, 2015).

This paper mainly aims to study different strategies for elastostatic calibration. The study was based on several measurement point locations, such as on the end-effector, after the second joint, on the robot arm, and after the forth joint. Selecting several measurement points might give some additional possibilities for robot calibration. To enhance the validity of presented analysis, we are comparing two different industrial robots. These robots have different joint compliance to analyze the suggested identification strategies in details. Hence, their joints have different impacts on the resulting accuracy and require additional investigation.

[a] https://orcid.org/0000-0002-7582-3517
[b] https://orcid.org/0000-0002-2244-1849

516

2 PROBLEM STATEMENT

In this work, the simulation study was based on the serial industrial manipulator Kuka KR-270 R-2700 and Fanuc r2000ic 165F (Fig. 1). These manipulators have similar kinematics structures but different joint compliance and link lengths (Klimchik et al., 2017). Basically, the classical identification is based on measuring points on the end-effector. The classical approach can calibrate all parameters at once. Unfortunately, the classical identification does not allow to identify joint parameters separately and may lead to a mutual balancing of the errors in the identified parameters. To overcome this limitation, we introduced and analysed several new measurement points. This analysis allowed us to decouple robot parameters and calibrate them more accurately (Jiang et al., 2020). In our study, both robots contained four reference points corresponding to different kinematics models: $2DoF$, $3DoF$, $4DoF$ and $6DoF$ (full) (see Fig. 2).

(a) Kuka KR-270 R-2700.   (b) Fanuc r2000ic 165F.
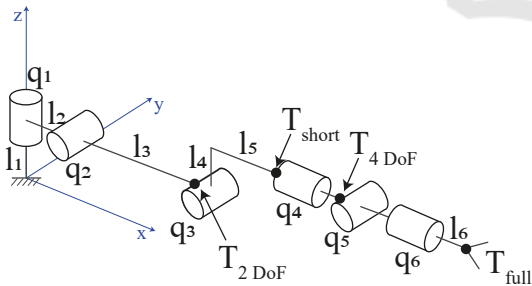
Figure 1: Robots under study.

Figure 2: Equivalent kinematics scheme of a serial industrial robot.

These points theoretically allow us to identify separately parameters of robot joint elasticity. In addition, these points also may achieve additional benefits. Therefore, we tested the following identification strategies:

1. **6DoF**. The identification algorithm considered the full kinematics ($\mathbf{T}_{full}$) and identified full vector of elastic parameters $\mathbf{c}$ at once. This algorithm required the data from the robot configuration $\mathbf{q}_i$,

measured position of the end-effector $\mathbf{p}^i_{full}$ and the values of applied wrenches $\mathbf{w}_i$.

2. **6DoF after 3DoF**. At the first step, we identified the first three elements of vector $\mathbf{c}$ using three DoF kinematics. At the second step, we used vector $\mathbf{c}$ as the initial condition and identified full vector $\mathbf{c}$ (wrist elasticity) using full kinematics. This algorithm required the data from the robot configuration $\mathbf{q}_i$, measured position for the three DoF kinematics $\mathbf{p}^i_{3\ DoF}$ and end-effector $\mathbf{p}^i_{full}$, as well as the values of applied wrenches $\mathbf{w}_i$.

3. **4-6DoF after 3DoF**. At the first step, we identified the first three elements of vector $\mathbf{c}$ using three DoF kinematics. At the second step, we identified the last three elements of vector $\mathbf{c}$ using the full kinematics. This algorithm required the data from the robot configuration $\mathbf{q}_i$, measured position for the 3 DoF kinematics $\mathbf{p}^i_{3\ DoF}$ and end-effector $\mathbf{p}^i_{full}$, as well as the values of applied wrenches $\mathbf{w}_i$.

4. **6DoF after 3+3DoF**. The identification algorithm considered the kinematics ($\mathbf{T}_{full}$) and identified the full vector of elastic parameters $\mathbf{c}$ at once. This algorithm used the vector $\mathbf{c}$ from "4-6DoF after 3DoF" strategy as initial condition for calibration. This algorithm required the data from the robot configuration $\mathbf{q}_i$, measured position for the three DoF kinematics $\mathbf{p}^i_{3\ DoF}$ and end-effector $\mathbf{p}^i_{full}$, as well as the values of applied wrenches $\mathbf{w}_i$.

5. **3+6DoF comb**. The identification algorithm considered the full kinematics ($\mathbf{T}_{full}$) and three DoF kinematics ($\mathbf{T}_{3\ DoF}$) simultaneously. Selected kinematics is used to identify the full vector of elastic parameters $\mathbf{c}$ at once. This algorithm required the data from the robot configuration $\mathbf{q}_i$, measured position for the three DoF kinematics $\mathbf{p}^i_{3\ DoF}$ and end-effector $\mathbf{p}^i_{full}$, as well as the values of applied wrenches $\mathbf{w}_i$.

6. **4-6DoF after 6+3DoF**. The identification algorithm considered the full kinematics ($\mathbf{T}_{full}$) and identified the last three elements of vector of elastic parameters $\mathbf{c}$ at once. This algorithms used the full vector $\mathbf{c}$ from "3DoF + 6DoF comb" strategy as initial condition for calibration. The algorithm required the data from the robot configuration $\mathbf{q}_i$, measured position for the three DoF kinematics $\mathbf{p}^i_{3\ DoF}$ and end-effector $\mathbf{p}^i_{full}$, as well as the values of applied wrenches $\mathbf{w}_i$.

7. **3-6DoF after 2DoF**. At the first step, we identified the first two elements of vector $\mathbf{c}$ using two DoF kinematics. At the second step, we identified the last four elements of vector $\mathbf{c}$ using the

full kinematics ($\mathbf{T}_{full}$). This algorithm required the data from the robot configuration $\mathbf{q}_i$, measured position for the two DoF kinematics $\mathbf{p}^i_{2\ DoF}$ and end-effector $\mathbf{p}^i_{full}$, as well as the values of applied wrenches $\mathbf{w}_i$.

8. **5-6DoF after 4DoF**. At the first step, we identified the first four elements of vector $\mathbf{c}$ using four DoF kinematics. At the second step, we identify last two elements of vector $\mathbf{c}$ using the full kinematics ($\mathbf{T}_{full}$). This algorithm required the data from the robot configuration $\mathbf{q}_i$, measured position for the four DoF kinematics $\mathbf{p}^i_{4\ DoF}$ and end-effector $\mathbf{p}^i_{full}$, as well as the values of applied wrenches $\mathbf{w}_i$.

However, it is not clear which strategy will achieve the most accurate robot model parameters identification and the highest robot precision accuracy after calibration. What is more, it is not evident how the selected model and its reduction effect the calibration accuracy. Hence, let us formulate several research questions which we addressed in this study.

RQ1: How does the model complexity affect the identification accuracy?

RQ2: How should we determine and introduce measurement points?

RQ3: Which number of reference point location for different kinematics models is able to achieve the accurate robot model parameters identification and the highest robot precision accuracy after calibration?

RQ4: How should we evaluate the efficiency of elastostatic calibration?

During this work every strategy was validated by 1000 different initial random seed configuration. The results present mean values along with all different initial random seed configurations. Moreover, we compared the described strategies for different noise both for position and orientation values. This noise was randomly normal (Gaussian) distributed noise without any shift of its mean. We also conducted several experiments with different standard deviation values: 0 m (or rad), $5 * 10^{-5}$ m (or rad), $1 * 10^{-4}$ m (or rad), $2 * 10^{-4}$ m (or rad) and $5 * 10^{-4}$ m (or rad). We selected such noise value based on robot parameters, especially repeatability. This value was about 60 μm for the selected robots. The noise value was also connected with measurement system accuracy, for example, a laser tracker had an accuracy of about 16 μm. Therefore, the selected noise was going to validate the identification approaches with similar noise impact as experimental validation on the real system.

For every robot configuration during simulation analysis, we applied the randomly generated force ($|\mathbf{F}| = 1000$ N) with a randomly generated direction. The force application point was shifted by 0.5 m along the Y axis. This offset was required to identify the last joint stiffness.

3 BENCHMARK EXAMPLE

The experiments were based on the "KUKA KR-270 R-2700" and "Fanuc R2000ic-165F" industrial manipulators. They both have similar kinematics scheme (see Fig. 2). Its 6DoF or full ($\mathbf{T}_{full}$), 2DoF kinematics ($\mathbf{T}_{2\ DoF}$), 3DoF kinematics ($\mathbf{T}_{3\ DoF}$) and 4DoF kinematics ($\mathbf{T}_{4\ DoF}$) can be computed as follows:

$$\mathbf{T}_{2\ Dof} = \mathbf{T}_{base}\mathbf{T}_z^{l_1}\mathbf{R}_z^{q_1}\mathbf{R}_z^{\theta_1}\mathbf{T}_x^{l_2}\mathbf{R}_y^{q_2}\mathbf{R}_y^{\theta_2}\mathbf{T}_x^{l_3}\mathbf{T}_{tool}^2 \quad (1)$$

$$\mathbf{T}_{3\ Dof} = \mathbf{T}^*_{2\ Dof}\mathbf{R}_y^{q_3}\mathbf{R}_y^{\theta_3}\mathbf{T}_z^{l_4}\mathbf{T}_x^{l_5}\mathbf{T}_{tool}^3 \quad (2)$$

$$\mathbf{T}_{4\ DoF} = \mathbf{T}^*_{3\ Dof}\mathbf{R}_x^{q_4}\mathbf{R}_x^{\theta_4}\mathbf{T}_{tool}^4 \quad (3)$$

$$\mathbf{T}_{full} = \mathbf{T}^*_{4\ DoF}\mathbf{R}_y^{q_5}\mathbf{R}_y^{\theta_5}\mathbf{R}_x^{q_6}\mathbf{R}_x^{\theta_6}\mathbf{T}_x^{l_6}\mathbf{T}_{tool}^6 \quad (4)$$

where q_i is the value of ith joint, θ_i is the value of ith virtual joint, l_i represents i^{th} link length and $\mathbf{R}_x$, $\mathbf{R}_y$, $\mathbf{R}_z$, $\mathbf{T}_x$, $\mathbf{T}_y$, $\mathbf{T}_z$ are elementary homogeneous transformation matrices. The matrices $\mathbf{T}^*_{2\ Dof}$, $\mathbf{T}^*_{3\ Dof}$, $\mathbf{T}^*_{4\ Dof}$ represent matrices $\mathbf{T}_{2\ Dof}$, $\mathbf{T}_{3\ Dof}$, $\mathbf{T}_{4\ Dof}$ respectively without tool transformation. Here $\mathbf{T}^j_{tool}, (j \in \{2,3,4,6\})$ describe measurement points transformations, $\mathbf{T}_{base}$ describes the base transformation. For simplicity, during the experiments $\mathbf{T}_{base}$ and $\mathbf{T}^j_{tool}$ were equal to identity matrix.

Any identification technique requires Jacobian matrices concerning the set of unknown parameters. The Jacobians concerning virtual joint variables θ was computed using Screw Theory (Jazar, 2022) for all models in this study.

Furthermore, we should describe the parameters of the robot. Both robots had similar kinematic structures and elastostatic models. They had different links length and equivalent joint compliances (see Table 1 for details). We selected robots with a similar structure to compare their difference in calibration accuracy.

4 IDENTIFICATION PROCEDURE

First, we selected an elastostatic model of a serial manipulator (Klimchik et al., 2017). So, we had to

Table 1: Equivalent joint compliances.

Robot	joint compliances, $\mu m/N$					
	c_1	c_2	c_3	c_4	c_5	c_6
Kuka	0.54	0.29	0.42	2.79	3.48	2.07
Fanuc	1.23	0.37	0.46	2.68	2.70	2.72

choose from several modeling approaches: Matrix Structural Analysis (MSA), Finite Elements Analysis (FEA), and Virtual Joint Modeling (VJM). Their advantages and disadvantages have been presented many times (Pashkevich et al., 2009; Deblaise et al., 2006; Quennouelle and Gosselin, 2008; Piras et al., 2005; Chen and Kao, 2000; Marie et al., 2013). Here, we chose the VJM modeling since it used the most appropriate method for the considered problem. In VJM modeling, the manipulator was presented as a sequential of rigid and elastic components: a fixed "Base", several flexible actuated joints "Ac", some flexible "Links" and an "End-effector". According to this method, the model of every link had to be extended by adding six DoF springs. We also had to add one DoF spring for every joint (Dumas et al., 2011; Kövecses and Angeles, 2007; Klimchik et al., 2012). Fig. 3 describes the elasticity of the related links/joints. Additionally, we extended the reduced VJM model only by adding one DoF spring after every joint.

Figure 3: VJM scheme of the robot.

With this method, every link was represented as a thick-walled beam. What is more, we had to extend the robot kinematics transformation by adding $\mathbf{T}_{6D}^{\theta_{1-6}}$, where $\mathbf{T}_{6D}^{\theta_{1-6}}$ is computed as follows:

$$\mathbf{T}_{6D}^{\theta_{1-6}} = \mathbf{T}_x^{\theta_1}\mathbf{T}_y^{\theta_2}\mathbf{T}_z^{\theta_3}\mathbf{R}_x^{\theta_4}\mathbf{R}_y^{\theta_5}\mathbf{R}_z^{\theta_6} \qquad (5)$$

Generally, this model contained numerous variables that cannot be strictly identified. Hence, we had to use the reduced VJM model. According to this technique, the rigid model had to be extended by adding one DoF spring followed by every joint as shown in Fig. 3.

The robot deflection depended on the configuration $\mathbf{q}$, while the applied wrench $\mathbf{w}$ of the serial manipulator for the given configuration was computed as follows

$$\mathbf{w} = \mathbf{K}_c\delta\mathbf{t} \qquad (6)$$

where $\mathbf{K}_c$ is the Cartesian stiffness matrix, $\delta\mathbf{t}$ is the

end-effector deflection (Salisbury, 1981; Klimchik et al., 2014).

The virtual joints displacement was found by the following equation:

$$\theta = \mathbf{K}_\theta^{-1}\mathbf{J}_\theta^T\mathbf{w} \qquad (7)$$

where $\mathbf{J}_\theta$ is the Jacobian matrix with respect to virtual joints θ that depends on the configuration $\mathbf{q}$ and $\mathbf{K}_\theta$ is the aggregated spring stiffness matrix of the size 6×6. This matrix describes the elastostatic properties of the manipulator links/joints.

To generate a simulation dataset, we used the above method. Here, wrench direction was randomly computed, but the applied force was constant ($|\mathbf{F}| = 1000$ N). Using computed θ and robot kinematics transformation we determined the ideal robot position ($\mathbf{p}_{init}$) which all identification strategies should achieve. Here, all required values were computed and the dataset might be stored.

In practice, $\mathbf{K}_\theta$ matrix was unknown and had to be found by any identification technique. Basically, identification required a dataset with several measured configurations, points, and applied wrench. Therefore, we can write the elastostatic model for the ith experiment as

$$\delta\mathbf{t}_i = \mathbf{J}_{\theta,i}\mathbf{K}_\theta^{-1}\mathbf{J}_{\theta,i}^T\mathbf{w}_i \qquad (8)$$

where, $\delta\mathbf{t}_i$ is end-effector displacement in the ith experiment and $\mathbf{w}_i$ is corresponding external wrench applied to the manipulator end-effector. The elastostatic model can be rewritten to show the connection between known and unknown parameters as follows:

$$\delta\mathbf{t}_i = \mathbf{A}_i\mathbf{c} \qquad (9)$$

where the vector $\mathbf{c}$ collects all unknown compliance coefficients and

$$\mathbf{A}_i = [\mathbf{J}_{i,1}\mathbf{J}_{i,1}^T\mathbf{w}_i, \mathbf{J}_{i,2}\mathbf{J}_{i,2}^T\mathbf{w}_i, \ldots, \mathbf{J}_{i,m}\mathbf{J}_{i,m}^T\mathbf{w}_i] \quad (10)$$

Here $\mathbf{J}_{i,j}$ represents columns of the Jacobian matrix $\mathbf{J}_{\theta,i} = [\mathbf{J}_{i,1}, \mathbf{J}_{i,2}, \ldots, \mathbf{J}_{i,n}]$.

The identification approach can be represented as the optimization problem based on the calibration requires several experiments. The solution of the described problem can be represented as follows:
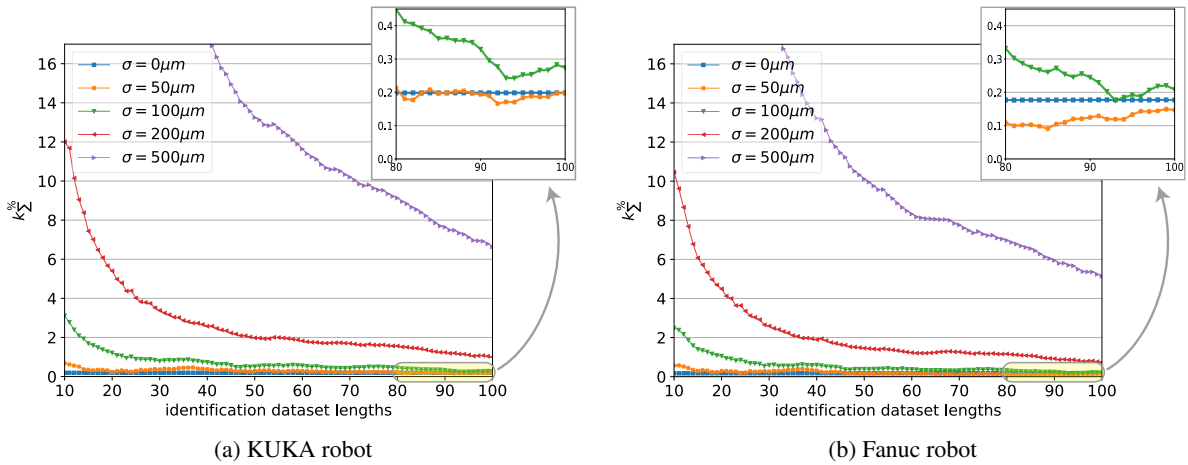
$$\hat{\mathbf{c}} = (\sum_{i=1}^{n}\mathbf{A}_i^T\mathbf{A}_i)^{-1}(\sum_{i=1}^{n}\mathbf{A}_i^T\delta\mathbf{t}_i) \qquad (11)$$

where n is the number of experiments.

5 ANALYSIS

To compare the described algorithms, let us introduce that the resulting $\mathbf{K}_\theta^c$ was computed by mean computing along 1000 experiments per dataset length (ds):

$$\mathbf{K}_\theta^c = diag(k_1^c, k_2^c, k_3^c, k_4^c, k_5^c, k_6^c) \qquad (12)$$

(a) KUKA robot

(b) Fanuc robot

Figure 4: Noise impact analysis for the **6DoF** identification strategy.

where diagonal element contains identified stiffness values for each robot joint. To describe the accuracy of computed parameters and taking into account that we know ideal values, it is more indicative to compare parameters in percent:

$$\delta k_i^\% = \frac{k_i^{comp} - k_i^{init}}{k_i^{init}} * 100\% \qquad (13)$$

where k_i^{init} is initial robot joint stiffness. Unfortunately, some values might be decoupled along with joints stiffness identification when joints were allocated along the same axis. Hence, to neglect this problem the result combined into single value:

$$k_\Sigma^\% = \sum_{i=1}^{6} \delta k_i^\% \qquad (14)$$

The following identification strategies results were compared with respect to computed single value $k_\Sigma^\%$.

Another method to compare considered strategies was achieved by deviation comparison.

$$dev(ds) = mean\left(\frac{1}{1000} \sum_{i=1}^{1000} (\mathbf{p}(ds)_{comp}^i - \mathbf{p}(ds)_{init}^i)\right) \qquad (15)$$

where ds is current dataset length value, $\mathbf{p}(ds)_{comp}^i$ is computed end-effector position after selected calibration strategy, $\mathbf{p}(ds)_{init}^i$ is initial simulated end-effector position before calibration. The presented metric $dev(ds)$ will be able to analyze more important metric such as resulting robot accuracy. Initial deviations are presented in Table 2 for both robots before any calibration technique. What is more, "Kuka extended" contained the deviation results for the Kuka robot where the full VJM model was used during dataset generation.

Firstly, we had to select the most representable noise value. Fig. 4 demonstrates the achieved calibration results for the **6DoF** identification strategy along

Table 2: Initial end-effector deviation value for both robots before calibration.

| Robot	accuracy, *mm*		
	mean	std	max
Kuka	0.929	0.636	2.864
Fanuc	1.497	1.487	9.516
Kuka extended	1.749	1.116	4.743

with different noise values for both robots. The values of 0 *μm*, 50 *μm* and 100 *μm* demonstrated similar results which tend to zero. Hence, their selection was not representable to compare different identification strategies. Otherwise, 500 *μm* noise demonstrated a lot of impacts from this noise. Hence, 500 *μm* noise value did not tend to appropriate robot calibration results. Therefore, the following comparison was done concerning 200 *μm* noise value. The classical **6DoF** strategy can achieve identification accuracy of less than 2 *μm* for both robots with less than 50 configurations in the dataset. This result is less than robot repeatability, hence, it will produce a lower impact on robot positioning accuracy.

Secondly, **6DoF**, **6DoF after 3DoF** and **6DoF after 3+3DoF** strategies demonstrates the same results. They were able to achieve the following joint compliance with 20 configurations in the dataset presented in Table 3. Generally, **6DoF** strategy seemed to achieve the result under any default conditions, no matter which initial stiffness matrix selected, and which initial thetas had been chosen.

Table 4 and Fig. 5 demonstrate the comparison of the achieved calibration results for the selected noise. These metrics were able to demonstrate that **4-6DoF after 6+3DoF** strategy was more accurate for both robots for any metric. **3+6DoF comb** strategy was able to achieve similar robot precision as the previous
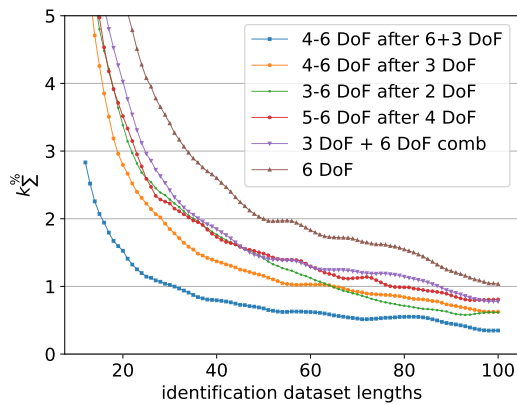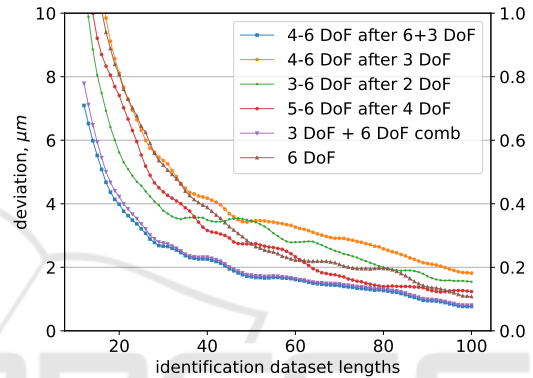
(a) Joint stiffness persantage difference for KUKA robot
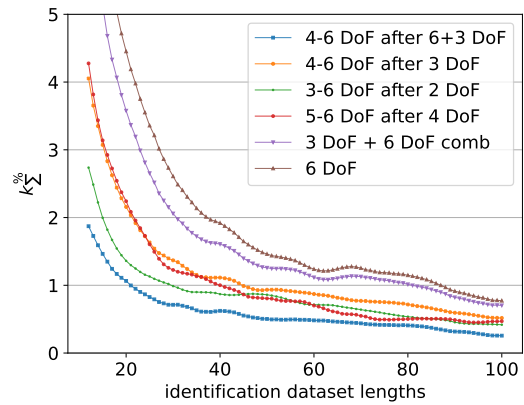
(b) Joint stiffness persantage difference for Fanuc robot
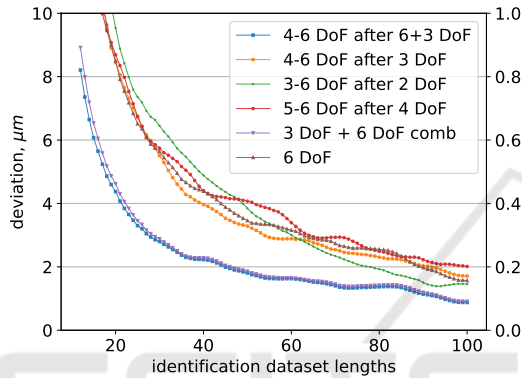
(c) Resulting deviation mean value for KUKA robot

(d) Resulting deviation mean value for Fanuc robot

Figure 5: Achieved results comparison for the noise 200 μm for robot calibration identification strategies.

Table 3: Achieved joint compliances values, $\mu m/N$.

Robot	joint compliances, $\mu m/N$					
	c_1	c_2	c_3	c_4	c_5	c_6
Kuka	0.538	0.287	0.414	2.774	3.464	2.047
Fanuc	1.233	0.370	0.455	2.663	2.667	2.694

one. The **4-6DoF after 6+3DoF** and **3+6DoF comb** identification strategies were at least 1.86 times more accurate for the resulting deviation metric than the classical **6DoF** identification. Unfortunately, **3+6DoF comb** strategy produced 2.75 times less precise results for exact joint compliance calibration than **4-6DoF after 6+3DoF** strategy. Other strategies' results were strictly dependent on the selected robot. The **3-6DoF after 2DoF** strategy could calibrate the Fanuc robot exact joint compliance within 30 configurations, but this strategy was not so accurate for the Kuka robot. During these comparisons, the Fanuc robot achieved more accurate results for any metric than the Kuka robot.

We also compared how residuals parameters had been affected by the robot precision after any cali-

bration. This experiment was done for Kuka robots modeling. The resulting accuracy was lower than 366 μm for any identification strategy with the noise of 200 μm. Therefore, the residuals parameters had a lot of impact on the resulting robot accuracy and selecting appropriate number or residual parameters required to have an accurate robot model. In this case, acceptable results could also be achieved.

Despite the benefits, the developed approaches had certain limitations. Firstly, different robots did not achieve similar results. This problem required analyzing how robot model parameters such as joint compliance and any geometrical parameters were influenced by the resulting robot accuracy (Klimchik et al., 2017; Klimchik and Pashkevich, 2017).

Secondly, the robot configurations were selected randomly. Optimal selection of measurement poses might increase resulting robot accuracy. Optimal selection of measurement poses does not have a lot of impact on results because all experiments were done with 1000 iterations. Hence, identification strategies were compared more clearly.

Table 4: Comparison analysis for the noise 200 μm for robot calibration identification strategies.

Strategy	Robot	Metric			
		$k_{\Sigma}^{\%}(20)$, %	$k_{\Sigma}^{\%} = 1\%$	$dev(20)$, μm	$dev = 2\mu m$
4-6DoF after 6+3DoF	Kuka	1.471	31	4.229	45
	Fanuc	1.036	22	3.867	46
4-6DoF after 3DoF	Kuka	2.743	66	8.206	90
	Fanuc	2.107	46	7.860	95
3-6DoF after 2DoF	Kuka	3.411	65	9.594	77
	Fanuc	1.379	30	5.592	80
5-6DoF after 4DoF	Kuka	3.485	76	8.680	100
	Fanuc	2.175	39	7.332	64
3+6DoF comb	Kuka	4.049	87	4.507	46
	Fanuc	3.633	82	4.143	46
6DoF	Kuka	5.405	100	8.386	89
	Fanuc	4.494	87	7.921	72

$k_{\Sigma}^{\%}(20)$ demonstrates how precise exact joint compliance values can be achieved with 20 configurations.

$k_{\Sigma}^{\%} = 1\%$ demonstrates how many configurations are required to achieve quite accurate joint compliance values. In this case robot should achieve not more that 1% for $k_{\Sigma}^{\%}$ metric.

$dev(20)$ demonstrates how accurate robot precision can be achieved with 20 configurations.

$dev = 2\mu m$ demonstrates how many configurations are required to achieve robot precision less than 2 μm.

6 CONCLUSION

The paper presents the simulation study on robot calibration approaches. Several new assumptions were tested while the analysis. The achieved results led to the following conclusions concerning the formulated hypothesis:

1. Selecting an appropriate model affects the identification accuracy. The reduced model was able to compensate 80% of joint and link elasticity. In the case if link elasticity is negligibly small the model was able to compensate 99% of compliance errors. The presented comparison was made for 20 measurement configurations in the dataset. Therefore, selecting an appropriate model can increase robot accuracy more precisely.

2. Select additional points which are visible during experimental validation demonstrated more accurate results. The exact point location requires additional study because of the tendency that point location depends on robot parameters.

3. We discovered that combining several datasets during identification is able to achieve more accurate results. This result is caused by partially increasing the dataset used for identification. In particular, we used two-point position measures instead of one point for every configuration.

4. The robot accuracy may be measured through several metrics. Mostly, the results coincided with different metrics. The exact metric selection strictly depends on the required task. Nevertheless, the comparison of resulting robot end-effector displacement might be the primary way to evaluate the efficiency of elastostatic calibration.

In the future, the developed methodology will be focused on comparing geometric and elastostatic robot parameter to analyze how the robot parameters influence the resulting calibration accuracy.

ACKNOWLEDGEMENTS

REFERENCES

Chen, S.-F. and Kao, I. (2000). Conservative congruence transformation for joint and cartesian stiffness matrices of robotic hands and fingers. *I. J. Robotic Res.*, 19:835–847.

Daney, D. and Emiris, I. (2001). Robust parallel robot calibration with partial information. volume 4, pages 3262–3267.

Deblaise, D., Hernot, X., and Maurine, P. (2006). A systematic analytical method for pkm stiffness matrix calculation. pages 4213 – 4219.

Driels, M., Swayze, W., and Potter, S. (1993). Full-pose calibration of a robot manipulator using a coordinate-measuring machine. *The Inter. J. of Advanced Manufacturing Technology*, 8:34–41.

Dumas, C., Caro, S., Garnier, S., and Furet, B. (2011). Joint stiffness identification of six-revolute industrial serial robots. *Robot. Comput.-Integr. Manuf.*, 27:881–888.

Elatta, A., Gen, L., Zhi, F., Daoyuan, Y., and Fei, L. (2004). An overview of robot calibration. *Information Technology J.*, 3:74–78.

Gonzalez, M. K., Theissen, N. A., Barrios, A., and Archenti, A. (2022). Online compliance error compensation system for industrial manipulators in contact applications. *Robot. Comput.-Integr. Manuf.*, 76:102305.

Hage, H. (2012). Identification and physical simulation of a stäubli tx90 robot during high-speed milling.

Jazar, R. (2022). *Theory of Applied Robotics: Kinematics, Dynamics, and Control (3rd Edition)*. Springer.

Jiang, Z., Huang, M., Tang, X., and Song, B. (2020). Observability index optimization of robot calibration based on multiple identification spaces. *Autonomous Robots*, 44:1029–1046.

Jin, J. and Gans, N. (2015). Parameter identification for industrial robots with a fast and robust trajectory design approach. *Robot. Comput.-Integr. Manuf.*, 31:21–29.

Joubair, A., Slamani, M., and Bonev, I. (2012). Kinematic calibration of a five-bar planar parallel robot using all working modes. *Robot. Comput.-Integr. Manuf.*, 29.

Kamali, K. and Bonev, I. (2019). Optimal experiment design for elasto-geometrical calibration of industrial robots. *IEEE/ASME Trans. on Mech.*, 24:2733–2744.

Klimchik, A., Ambiehl, A., Garnier, S., Furet, B., and Pashkevich, A. (2016). Experimental study of robotic-based machining. *IFAC-PapersOnLine*, pages 174–179.

Klimchik, A., Ambiehl, A., Garnier, S., Furet, B., and Pashkevich, A. (2017). Efficiency evaluation of robots in machining applications using industrial performance measure. *Robot. Comput.-Integr. Manuf.*, 48:12–29.

Klimchik, A., Bondarenko, D., Pashkevich, A., Briot, S., and Furet, B. (2014). Compliance error compensation in robotic-based milling. *Informatics in Control, Automation and Robotics*, 283.

Klimchik, A., Furet, B., Caro, S., and Pashkevich, A. (2015). Identification of the manipulator stiffness model parameters in industrial environment. *Mech. Mach. Theory*, 90:1–22.

Klimchik, A. and Pashkevich, A. (2017). Serial vs. quasi-serial manipulators: Comparison analysis of elasto-static behaviors. *Mech. Mach. Theory*, 107:46–70.

Klimchik, A., Pashkevich, A., Caro, S., and Chablat, D. (2012). Stiffness matrix of manipulators with passive joints: Computational aspects. *Robot. IEEE Trans. on*, 28:955–958.

Kövecses, J. and Angeles, J. (2007). The stiffness matrix in elastically articulated rigid-body systems. *Multibody System Dynamics*, 18:169–184.

Li, Z., Li, S., and Luo, X. (2021). An overview of calibration technology of industrial robots. *IEEE/CAA J. of Automatica Sinica*, 8:23–36.

Ma, L., Bazzoli, P., Sammons, P., Landers, R., and Bristow, D. (2017). Modeling and calibration of high-order joint-dependent kinematic errors for industrial robots. *Robot. Comput.-Integr. Manuf.*, 50.

Mamedov, S., Popov, D., Mikhel, S., and Klimchik, A. (2018). Compliance error compensation based on reduced model for industrial robots. pages 190–201.

Marie, S., Courteille, E., and Maurine, P. (2013). Elasto-geometrical modeling and calibration of robot manipulators: Application to machining and forming applications. *Mech. Mach. Theory*, 69:13–43.

Nguyen, V. L., Kuo, C.-H., and Lin, P. T. (2022). Compliance error compensation of a robot end-effector with joint stiffness uncertainties for milling: An analytical model. *Mech. Mach. Theory*, 170:104717.

Nubiola, A. and Bonev, I. (2013). Absolute calibration of an abb irb 1600 robot using a laser tracker. *Robot. Comput.-Integr. Manuf.*, 29:236–245.

Park, I.-W., Lee, B.-J., Cho, S.-H., Hong, Y.-D., and Kim, J.-H. (2012). Laser-based kinematic calibration of robot manipulator using differential kinematics. *Mech. IEEE/ASME Trans. on*, 17:1059–1067.

Pashkevich, A., Chablat, D., and Wenger, P. (2009). Stiffness analysis of overconstrained parallel manipulators. *Mech. Mach. Theory*, 44:966–982.

Piras, G., Cleghorn, W., and Mills, J. (2005). Dynamic finite-element analysis of a planar high-speed, high-precision parallel manipulator with flexible links. *Mech. Mach. Theory*, 40:849–862.

Qin, J., Léonard, F., and Abba, G. (2016). Real-time trajectory compensation in robotic friction stir welding using state estimators. *IEEE Trans. on Control Systems Technology*, 24:2207–2214.

Quennouelle, C. and Gosselin, C. (2008). *Stiffness Matrix of Compliant Parallel Mechanisms*, pages 331–341. Springer.

Renders, J.-M., Rossignol, E., Becquet, M., and Hanus, R. (1992). Kinematic calibration and geometrical parameter identification for robots. *Robot. and Automation, IEEE Trans. on*, 7:721 – 732.

Salisbury, J. (1981). Active stiffness control of a manipulator in cartesian coordinates. volume 1, pages 95 – 100.

Veitschegger, W. and Wu, C.-h. (1987). A method for calibrating and compensating robot kinematic errors. volume 4, pages 39 – 44.

Wu, L., Yang, X., and Chen, K. (2015a). A minimal poe-based model for robotic kinematic calibration with only position measurements. *IEEE Trans. on Automation Science and Eng.*, 12:758–763.

Wu, Y., Klimchik, A., Caro, S., Furet, B., and Pashkevich, A. (2015b). Geometric calibration of industrial robots using enhanced partial pose measurements and design of experiments. *Robot. Comput.-Integr. Manuf.*, 35.